

Exploration of the double-diffusive convection during dendritic solidification with a combined volume-averaging and cellular-automaton model

This article has been downloaded from IOPscience. Please scroll down to see the full text article.

2012 IOP Conf. Ser.: Mater. Sci. Eng. 33 012115

(<http://iopscience.iop.org/1757-899X/33/1/012115>)

View [the table of contents for this issue](#), or go to the [journal homepage](#) for more

Download details:

IP Address: 178.191.204.136

The article was downloaded on 31/05/2013 at 10:23

Please note that [terms and conditions apply](#).

Exploration of the double-diffusive convection during dendritic solidification with a combined volume-averaging and cellular-automaton model

A Kharicha, M Stefan-Kharicha, M Wu, A Ludwig

Chair for Simulation and Modelling of Metallurgical Processes, Dept. of Metallurgy, Univ. of Leoben, A-8700 Leoben, Austria

E-mail: abdellah.kharicha@notes.unileoben.ac.at

Abstract. A two-dimensional model is built and used to study thermo-solutal (double diffusive) convection generated during the solidification of a binary mixture in a rectangular enclosure cooled from bottom and side walls. In order to catch the smallest solute plumes scale the solidification model simulates directly the envelope of the columnar dendrites with a cellular automaton model. The mushy interior of the dendrite is modelled with a volume averaging method. The model predicts the occurrence of several flow regimes during solidification, such as turbulent, stratified and meandering flows. As a result or origin of the two dimensional meandering flow pattern, the concentration field is found to be organised in horizontal layers of uniform concentration. Those layers are separated by very thin boundary layers so that the concentration varies vertically in staircases.

1. Introduction

The study of double-diffusive natural convection has many environmental and industrial applications including oceanography, petrochemical applications processes, oil and gas extraction, and solidification processes. In a number of experimental and numerical studies, it has been shown that the interaction between thermal and compositional buoyancy, phenomena such as oscillatory flow, chaotic and turbulent flows can be generated. Turner [1] described double-diffusive convection as a phenomenon that happens when there are gradients of two or more properties with different molecular diffusivities. The double-diffusive instability represents an efficient phenomenon that releases potential energy stored in one of the density components, even when the density distribution is statically stable. There are mainly two types of double-diffusion, which are known as the plumes (or fingers) regime and the diffusive convection regime.

The plumes instability [2] appears as a close-packed array of up-and downward flowing convection cells which exchange large quantity of heat laterally, but only small amount of solute. This results in an advective transport of solute and, to a lesser extent, heat, in the vertical direction. This form of instability is, however, of limited interest, since diffusive oscillations are sometimes replaced by the relatively steady patterns, characterized by a layered distribution of temperature and (or) concentration [3]. Well-mixed layers separated by sharp diffusive interfaces are responsible for stair-like appearance of the temperature profiles in the central Arctic thermocline. Such profiles are referred to as thermohaline staircases. There exist numerous studies on formation of staircase-like structures. Its mathematical modelling, including fluid dynamics, and in oceanography is supported by many laboratory experiments with a large amount of experimental data [4-7]. Many aspects of the origin of

such structures, in spite of long history of its studies, are still unclear and are a subject for speculations.

During solidification, natural convection arises from the temperature and concentration gradients. Concentration gradients are caused by the preferential incorporation or rejection of solute element at the solid-liquid interface. Due to the fact that direct observation of solidification and convection is not possible in metallic alloys, many researchers in the field of metallurgy have used transparent analogue systems [8-10], such as ammonium chloride salt. Using such transparent analogues it has been possible to visualize the effects of the convections on the solidification pattern and the resulting macrosegregation. Using a shadowgraph method during the solidification of an ammonium chloride-water solution [8, 9] has described a variety of double-diffusive phenomena including plumes and layering. More recently PIV measurements of the flow velocity revealed the existence of a “meandering flow regime” [10]. The liquid was found to flow along a snaky path from the top of the cavity to the bottom near the mushy zone. The velocity was mainly horizontal in the bulk, the flow was downward only at the vicinity of the lateral mushy zones. A staircase layering of the concentration field could be at the possible origin of this snaky flow regime. Unfortunately the concentration field could not be directly observed.

Double diffusive phenomena considerably influence the local solidification rate and in some cases a part of the mushy region can even be re-melted [8-10]. Remelting is believed to be the most probable origin of the chimney (freckle). Worster [11] studied the linear instability of directional solidification. Assuming a simple equation for permeability, he demonstrated the existence of two modes of instability. At large wavelengths convection cells are able to penetrate deep into the mushy zone, while at shorter wavelengths the convection cells remain confined in the liquid region. The long wavelengths were assumed to be at the origin of chimneys. Modelling of the evolution of convection cells and chimneys demands an analysis that captures all nonlinearities in the governing equations.

Simulations of the double diffusive convection during solidification were performed for various alloy composition [12-14]. However the formation of plumes or layers could rarely be captured. The main reasons lie on the limited grid size, but also on the fact that variations of concentrations are generated at discrete positions separated by a typical distances which could be related to the primary arm spacing. In fact, solidification (or melting) introduces an additional parameter compared to studies related to oceanography where most of the analysis focuses simply on the mixing or formation of solute layers. During columnar solidification, if the density of the rejected solute is lower, each dendrite tip launches convective plumes into the upper liquid bulk region.

The present paper presents a numerical model which aims to study the generation of the “double diffusive turbulence” and the occurrence of layering as observed experimentally by Kharicha [10] in a thin enclosure (80 mm high, 100 mm wide, 10 mm thick). Since very small scale of the dendrite envelope needs to be captured, a cellular automaton model is employed. Evolution of the solid fraction in dendrites, the flow and the species transport are modelled with a volume averaging approach [15].

2. Numerical Model

The model describes conservation of mass, momentum, energy and species for a binary mixture, fluid-solid system. The shallow layer 2D model is assumed and the equations are written in terms of volume-averaged quantities. We assume that the total buoyancy is the sum of thermal and solutal buoyancies. The dendritic solidification model is divided in two parts. The first part aims to predict the large scale morphology of the solidification. It consists in using a tuned cellular automaton to model the dendrites envelope. The inner volume of the dendrite is not directly simulated but modelled as a mushy region. The model is based on the following assumptions: (1) no diffusion occurs in the solid phases, and the solute reaches local equilibrium concentration at the solid/liquid interface; (2) equiaxed crystals are neglected, no nucleation occurs in the bulk liquid, only the growth of the seeds placed at the cooled walls is considered.

2.1. Shallow layer model and volume-averaging equations

The volume shrinkage/expansion is ignored, and an incompressible Boussinesq approximation is employed to consider the thermo-solutal buoyancy. We assume a constant thermal α and solutal β expansion coefficient around the reference temperature T_0 and concentration C_0 . The 3D cell (geometry) is simplified as a 2D shallow layer. The mixture velocity \bar{u} and mixture temperature T are assumed to be parabolic within the thickness (d) of the cell. The 2D equations governing conservation of mass, momentum, energy and species concentration are written as follows:

$$\left. \begin{aligned} \frac{\partial(\rho_l \bar{u})}{\partial t} + \nabla \cdot (\rho_l \bar{u} \bar{u}) &= \nabla(\mu_l \nabla \bar{u}) - \nabla P + \rho_l f_l \bar{g} [\alpha(T - T_0) + \beta(C_1 - C_0)] - \frac{\mu_l}{\Pi} \bar{u} \\ \nabla \cdot \bar{u} &= 0 \end{aligned} \right\} \quad (1)$$

$$\frac{\partial(\rho_l f_l C_l)}{\partial t} + \nabla \cdot (\rho_l C_l \bar{u}) = \nabla \cdot (f_l \rho_l D_{eff} \nabla C_l) - \rho_s C_s \frac{\partial f_s}{\partial t} \quad (2)$$

$$\rho_s \frac{\partial f_s}{\partial t} = M_{CA} + M_{la} \quad (3)$$

$$\bar{\rho} C_p \frac{\partial T}{\partial t} + \bar{\rho} C_p \nabla \cdot (T \bar{u}) = \nabla(D_T \nabla T) + \rho_s L \frac{\partial f_s}{\partial t} - 2Q_{LG} \quad (4)$$

where $P, f_l, f_s, C_l, \rho_l, \rho_s, \mu_l$ are the static pressure, the liquid and solid fractions, the concentration of the solute (NH_4Cl), the liquid and solid densities, and the liquid viscosity. $\Pi, D_{eff}, D_T, \bar{\rho}, C_p, L$ are the local permeability, the effective solute diffusivity, the mixture heat conductivity, the mixture density, the mixture heat capacity, and the heat of fusion. M_{CA} is the mass transfer due to the growth of the dendrite envelop, M_{la} the mass transfer due to the growth of secondary arms, and Q_{LG} is the heat lost through the front and back glass.

The glasses temperature evolves according to the exchanged heat with the bulk liquid Q_{LG} and with the ambient air Q_{Air} :

$$\rho_G C_{p-G} \frac{\partial T_G}{\partial t} = \nabla(D_{T-G} \nabla T_G) + Q_{LG} - Q_{Air} \quad (5)$$

In the above equation ρ_G, C_{p-G}, D_{T-G} are the glass density, heat capacity, and heat conductivity. Q_{Air} is the heat lost (or gained) through contact with air. The heat exchange terms takes the form:

$$Q_{LG} = \frac{D_T}{2d^2} (T - T_G) \quad (6)$$

The exchange with air is modelled with a constant heat transfer coefficient h :

$$Q_{Air} = -h(T_G - T_{Ambient}) \quad (7)$$

The temperature of the ambient air is assumed to be constant and equal to 20°C.

2.2. Cellular Automaton model for the dendrites

The envelope of the dendrite is assumed to solidify a fixed quantity F_{Si} of solid. This quantity can represent the volume of solid contained in some primary and secondary tip length. Here F_{Si} is set to be equal to 3%, this means that when a cell has been crossed by the envelop surface, 97% of the cell is still liquid. The algorithm of envelope growth consists in stating that each cell has three possible states: liquid ($f_s = 0$), interface ($0 < f_s / F_{Si} < 1$), or mush ($f_s / F_{Si} > 1$).

At the interface the equilibrium liquid concentration C_L^i is defined as:

$$C_L^i = C_0 - \frac{1}{m_L} [T_L - \Gamma_i \bar{k} - T(t)] \quad (8)$$

Where T_L is the equilibrium liquidus temperature of the alloy, m_L the liquidus slope in the phase diagram, \bar{k} the mean curvature of the mush/liquid interface, Γ_i is a modified Gibbs-Thomson coefficient and C_0 is the initial concentration in the liquid. A nucleus that forms at a particular location will grow based on the growth velocity of the mush/liquid interface given by equation (9):

$$M_{CA} = V_n (\rho_l C_L^i - \rho_s C_S) F_{Si} = \begin{cases} M_{LGK} & (\bar{k} > 0.95 / \Delta x) \\ D_{eff} \rho_l F_{Si} \frac{C_l - C_L^i}{\Delta x} & (\bar{k} \leq 0.95 / \Delta x) \end{cases} \quad (9)$$

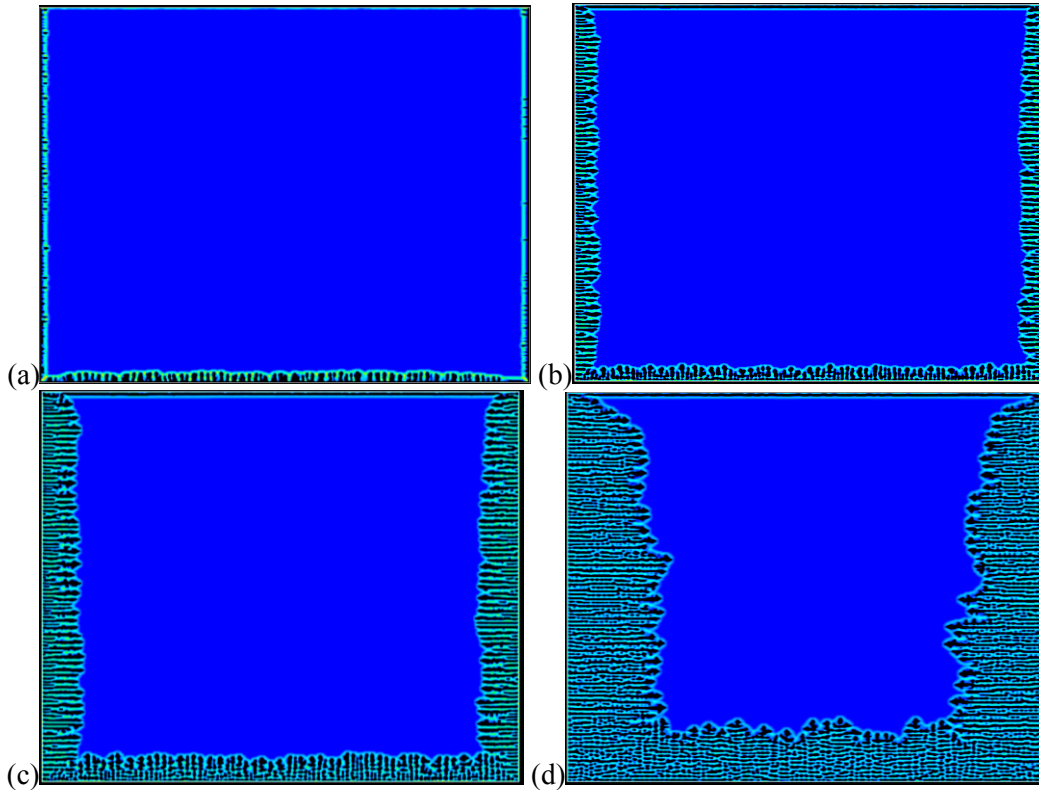


Figure 1. Evolution of the columnar dendrite envelope with time. a) beginning of the solidification (t~5 min); b) early stage of solidification (t~9 min); c) mid-stage of solidification (t~14 min); d) late stage (t ~30 min).

where V_n is the normal velocity of the interface, M_{LGK} is the species transfer, Δx the grid size, C_S the solute concentration in the solid of the interface, D_{eff} is the effective liquid solute diffusivity, \bar{n} the vector normal to the interface. Since grid size Δx is too large to resolve the dendrite tip, the mass transfer rate is artificially adapted so that V_n equals the Lipton-Glicksman-Kurz (LGK) solution for columnar tip growth. The cell in which the dendrite tip is located is identified by its high level of curvature almost equal to the maximum possible curvature for the present grid size ($\bar{k}_{max} \approx 1/\Delta x$). Outside the tip region, the growth is assumed to be controlled through diffusion. However since the cell size is coarse, the effective diffusivity of the solute must be increased by relatively large factor. In the present study the possibility of growth anisotropy due to crystallographic orientation is not expressively included, some anisotropy is naturally introduced by the grid orientation. The columnar dendrites modelled by the present CA model must achieve a defined tip velocity and a main primary arm spacing. The tip velocity is automatically fulfilled by the use of the LGK model. The primary arm spacing will depend on the proper choice of modelling parameters, for the present case is better to choose a combination which is not too far from the original physical parameters. We simply assume that the present dendrite grows as if the scale was N ($N=100$) times larger, so the curvature and the effective diffusivity equation (9) are simply multiplied by the same factor. The summary about physical and effective properties used in the present investigation, are presented in Table 1.

2.3. Mass transfer in the inner dendritic mushy region

For the process to be studied, the mushy region never solidifies completely. If we can imagine that the mesh topology can be represented as parallel or crossed cylindrical sticks, we can use the multiphase volume-averaging approaches developed by Wu et al. [15]. Originally this model was developed for periodic alignment of primary arm columnar trunks. Since the primary arm spacing λ_1 is already modeled with the cellular automaton model, the model of Wu et al.[15] is used in the present analysis with the secondary arms spacing λ_2 . The size of the sticks must represent an average of the secondary arms diameters. For the volume elements that has been passed by the envelop front, a diffusion-controlled growth model around cylindrical trunks is used. The growth velocity in the radial direction of such a cylindrical trunk is:

$$V_a = \frac{D_{eff}}{R_a} \frac{C_L^i - C_l}{C_L^i - C_s} \ln^{-1} \left(\frac{R_f}{R_a} \right) \quad (10)$$

where R_a is the average radius of the dendritic trunks, $R_f = \lambda_2 / \sqrt{\pi}$ is the maximum packing radius of a secondary dendrite arm trunk. For the sake of simplicity, the trunks are assumed to be parallel and staggered, so that the surface area of the secondary arm trunks per volume is $S_A = (4/\sqrt{3})\pi R_a / \lambda_2^2$.

The net volume-averaged mass-transfer rate for elements within the mushy region is:

$$M_{la} = V_a \left(\frac{4}{\sqrt{3}} \pi \frac{R_a}{\lambda_2^2} \right) \rho_s f_l \quad (11)$$

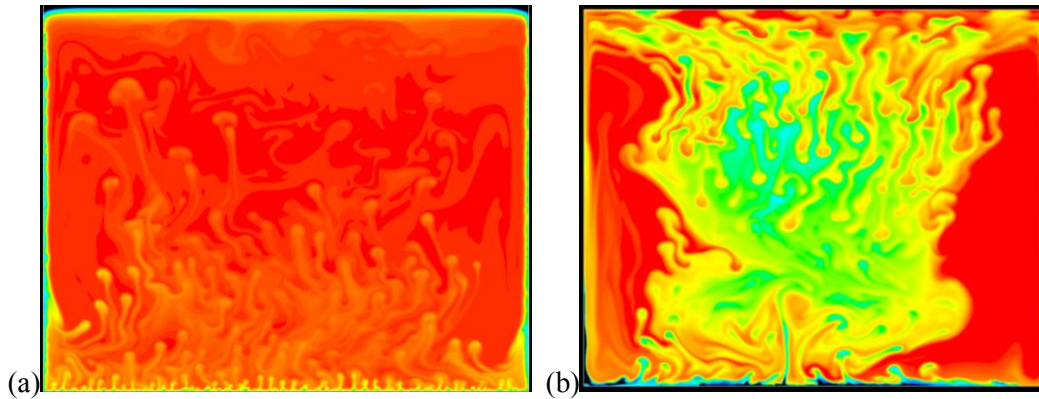


Figure 2. Concentration field. a) [0.29 wt.%, 0.3 wt.%] $t \sim 2$ min (not shown in Figure 1); b) [0.26 wt.%, 0.3 wt.%] $t \sim 5$ min (see Figure 1a).

2.4. Total Permeability

Permeability is typically modelled as varying with the solid fraction from zero at $f_s=0$ to infinity at $f_s=1$. In a shallow layer the permeability of the system includes the permeability of the shallow cell itself, $d^2/12$ [16]. The canonical choice for the mush permeability is the Kozeny-Carmen relationship. However by considering the morphology of the mush it is probably more appropriate to use the alternative form that represents a flow along or perpendicular to parallel cylinders in hexagonal configuration [17]:

$$\Pi_s = -\frac{4R_a^2}{32f_s} \left(\ln \frac{1}{f_s} - 1.497 + 2f_s - \frac{f_s^2}{2} - 0.739f_s^4 + \frac{2.534f_s^5}{1+1.2758f_s} \right) \quad (12)$$

The total effective permeability takes the form:

$$\Pi = \left(\frac{12}{d^2} + \frac{1}{\Pi_s} \right)^{-1} \quad (13)$$

2.5. Numerical method

The model was implemented within the commercial CFD software FLUENT. The time step used in the calculation depends on the maximum velocity of the liquid and of the maximum growth velocity of the dendrite envelop:

$$\Delta t = \frac{1}{5} \min\left(\frac{\Delta x}{U_{\max}}, \frac{\Delta x}{V_{\max}}, 10^{-2}\right) \quad (14)$$

In practice, it is the flow which limited most often the size of the time step. Typical calculation time for is in the order of 50-70 hours on an PC computer.

Table 1: Boundary conditions and effective parameters used for simulations

Property/Symbol	Value	Property/Symbol	Value
C_0	0.3 kg/kg	ρ_l	1078 kg/m ³
T_0	40°C	ρ_s	1500 kg/m ³
cooling rate	1.2 C/min	mixture $\bar{\rho}$	$\rho_l f_l + \rho_s f_s$
T_f	7 °C	mixture thermal conductivity, D_T	$0.54f_l + 2.2f_s$ W/m K
β_T	0.00021	glass thermal conductivity, D_{T_G}	0.96 W/m K
Δx	0.2 mm	L	3.5e5 W/kg
secondary arm spacing λ_2	0.1 mm	μ_l	0.0014
eff. solute diffusive coeff. D_{eff}	100*4.9e-9 m ² /s	C_p	1000 $f_l + 3500f_s$
eff. Gibbs Thomson coeff. Γ_i	5.05e-5 K m	C_{p_G}	500 W/kg/K
h	100 W/K m ²	C_s	1 kg/kg
β_c	-0.3	ρ_G	2500 kg/m ³
F_{Si}	0.03	liquidus slope, m_l	4.8 K/mass fraction

3. Results and discussion

The numerical results are presented in Figures 1- 4. Figure 5 presents selected experimental flow patterns obtained with a PIV technique. Four pictures representing the evolution in time of the dendrites envelopes shows a columnar-like type of growth (Figure 1). Before the beginning of solidification the temperature distribution shows the presence of temperature boundary layers at the cooling walls, which drives the flow in the direction of natural convection. The solidification is found to generate 4 different patterns of thermo-solutal convection, a regular plume regime, a chaotic regime, and two layered regimes.

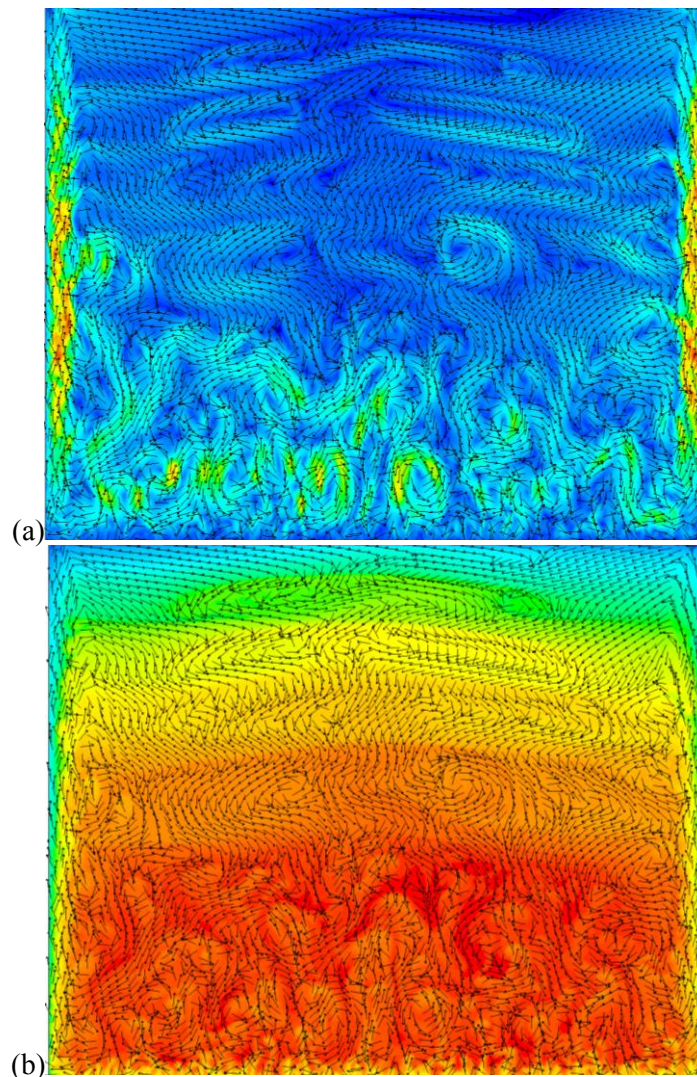


Figure 3. Velocity vectors during stratification of the concentration field $t \sim 9$ -15 minute. a) velocity magnitude and vectors [10^{-4} - 0.02 m/s]; b) velocity vectors and concentration field 0.2 wt% (blue) - 0.27 wt% (red).

At the start of solidification, the rejected solute disturbs the established thermo-buoyant convective flow by launching light solutal plumes (Figure 2a). The plume state displays two basic regimes. The initial one (Figure 2a) is dominated by the birth and rise of small plumes in vicinity of the bottom horizontal wall. During this early process the main flow path and bulk concentration stay almost unchanged. The duration is of the order of minutes.

The chaotic regime (Figure 2b and Figure 5a) is characterized by larger plumes generated within the liquid bulk and by an irregular formation of plumes near the horizontal solidification front. Due to the fast thermal diffusivity compared to the solutal one, the plumes generated in the liquid bulk consist of hot fluid with lower solute concentration. In opposite to previous regime large concentration gradient exists in the liquid bulk. During this regime no clear flow pattern can be observed, liquid flows successively in all directions at relatively high velocity magnitude. It can be assumed that this regime is the fruit of higher or balanced competition between thermal and solutal buoyancy. This unsteady behaviour changes the dynamic of plumes formation at the solidification front, typical distance between plumes seems to be no more related to the primary arm spacing as in early stage

(Figure 2a). The plumes are in fact emitted from an unstable and irregular boundary layer. The duration of this second regime is of the order of 10 minutes. In its course the bulk plume regime becomes increasingly disordered till it fades away giving birth to the stratified regimes.

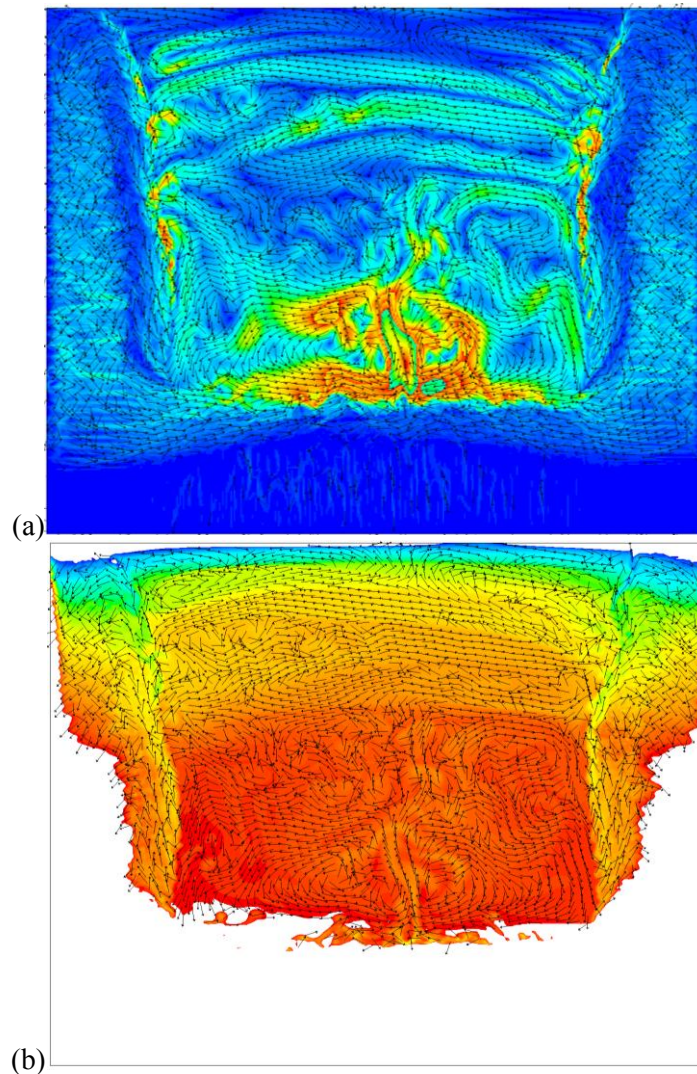


Figure 4. Velocity vectors during stratification of the concentration field $t \sim 12-45$ minutes. a) velocity magnitude and vectors [10^{-4} - 0.004 m/s]; (b) velocity vectors and concentration field 0.211 wt% (blue) - 0.22 wt% (red).

After the plume stages, comes a regime characterized by larger scale eddies (Figure 3 and 4). However the plumes generation is still present especially near the bottom solidification front. Progressively a stratification of the concentration field starts from the upper part of the cell. One or two layers were clearly observed during solidification by [8, 9] with shadography technique. Here up to 5 layers of quasi-uniform concentration were predicted (Figure 3b). Such layers are characterised by horizontal convective cells. During PIV experiment similar thin convection cells were observed (Figure 5b), unfortunately the concentration field could not be simultaneously measured. However, by superimposing the predicted velocity and concentration field (Figure 3b), we can assume that each of the horizontal cells is associated with a staircase of concentration. With time such convection cells layers merge into a single meandering flow path (Figure 4). Experimentally this path fills the liquid

region from left to right with typically 4 but up to 8 layers. In present simulations only 4 layers were formed (Figure 4a and b). It can be seen a good agreement between numerical and PIV results (Figure 5c).

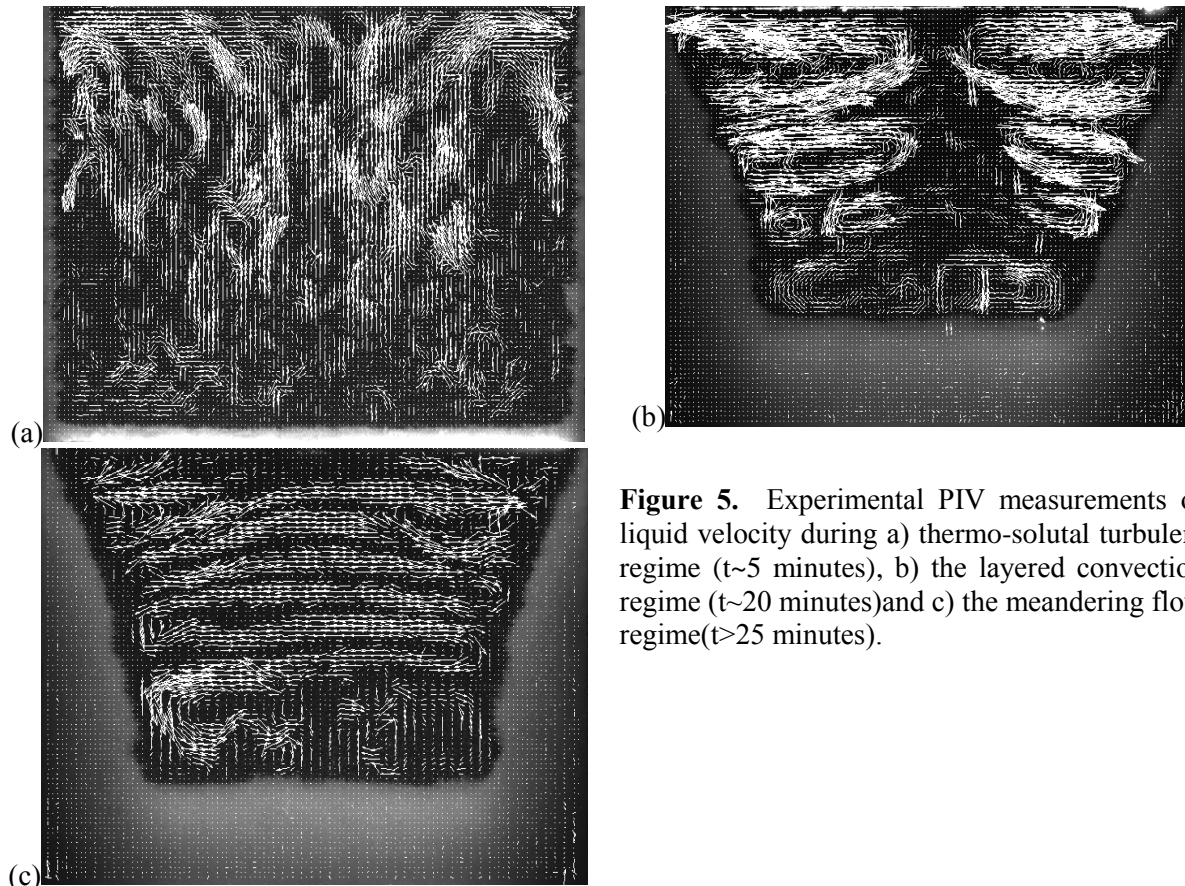


Figure 5. Experimental PIV measurements of liquid velocity during a) thermo-solutal turbulent regime ($t \sim 5$ minutes), b) the layered convection regime ($t \sim 20$ minutes) and c) the meandering flow regime ($t > 25$ minutes).

The predicted solidification front fits qualitatively with the observed one. The solidification starts from all the walls with a planar front (Figure 1a). The growth morphology changes quickly into cellular, and finally bifurcates into a columnar dendritic type. The fact that solidification was slower in the earlier stages at the vertical walls is attributed to the strong downwards jet flow which thins the heat boundary layers. Later the reorganisation of the flow, especially during the chaotic regime, redistributes the solute which then allows a faster solidification rate at the vertical walls. Solidification loses its symmetry during the stratified regimes (Figure 1d) which is not the case in the experiments (Figure 5). Since new nucleation during the process is not allowed during the growth it was not possible to simulate the change in direction of the growing dendrites with the constitutional temperature gradient. In the future this quality will be implemented within the model.

The importance of solutal buoyancy can be stated as follows: in the present system the ratio of solutal to thermal buoyancy effects ($\beta_c \Delta C / \beta_T \Delta T$) is of order of unity, whereas the same ratio can be an order of magnitude higher for many metal-alloy systems. It is clear that a stronger solutally driven convection can be expected in actual metal-alloy systems than in the NH_4Cl analogue. Moreover, solutal convection introduces kinetic energy at various wave lengths, which leads to the double diffusive chaos or turbulence. During solidification the smallest wave lengths are probably more related to the primary than to the secondary arm spacing. The present model predicted primary arm spacing larger but still in the same order as the observed ones ($\sim 1-3$ mm). For industrial cast system, it is not soon that the primary arm spacing will be simulated as it is with the present approach. This means that correct numerical predictions need either a grid size of λ_1 order, or the use of good closure laws. Unfortunately no universal closure laws exist which relates the thermo-solutal field to

the turbulence parameters. This closure problem is very well known by the oceanographic community which tries to predict and explain how layering in salt concentration can be generated at the scale of the ocean. Nevertheless, we believe that the present model can be used for scales where a single cellular automaton dendrite can represent several (N times) dendrites. Instead of introducing waves of λ_1 length as reality, the model will introduce waves of $N\lambda_1$ length. The number N can probably be as large as 10 or 100. In the field of numerical simulation using volume averaging techniques, grid independency is often required as a guaranty of quality. However, it is clear that in the present model the proper choice of F_{Si} , N , D_{eff} , and Γ_i is grid size dependent. Similarly than in the field of turbulence modeling, unless resolutions of the smallest scales are achieved, grid independent results are neither realizable nor desirable. What is desirable is the ability to catch new physical mechanisms which can hardly be predicted with classical volume averaged techniques. With the use of additional proper closure laws, the model might give in the future good predictions even for large scale solidification processes.

4. Conclusion

A numerical model is developed to study the double diffusive convection during solidification of a binary alloy. The model uses a cellular automaton approach to simulate the dendrite envelope. A volume average model is applied to tackle the solidification inside the dendrite envelope. It was shown that various flow phenomena are induced by the liquid density change ahead of the solidification front. Even if the shape of the solidification front is simple, the flow patterns are rather complex. It is predicted that during the solidification, solutal buoyancy has the potential to overcome thermal buoyancy at certain locations, giving rise to turbulent solute-driven vortices. In the later stage strong stratification of the concentration field occurs. Hydrodynamics, associated with these variations of solute in staircases, are characterised by thin convective layers or by a meandering flow. The liquid flow follows an almost horizontal snaky path from the top to the bottom of the cavity. During those layered paths the coupling of the fluid flow with the solid dissolution produces irregular patterns at the solid-liquid interface. Such complex phenomena are expected to be prominent in actual metal-alloy systems, so more effort must be made to explore double diffusive convection during solidification.

Acknowledgements

The research was funded by the Austrian Science Fund (FWF): P22614-N22.

References

- [1] Turner J S 1973 *Buoyancy Effects in Fluids* (Cambridge, England: Cambridge University Press)
- [2] Stern M E 1960 *Tellus* **12** 172-175
- [3] Prikasky I J Ph.D. Naval Postgraduate School Monterey, California 2007
- [4] Fernando H J S 1987 *J. Fluid Mech.* **182** 525-541
- [5] Fernando H J S 1989 *J of Physical Oceanography* **19** 1707-1715
- [6] Linden P F 1979 *Geophysical and Astrophysical Fluid Dynamics* **13** 3-23
- [7] Turner J S 1968 *J. Fluid. Mech.* **33** 183-200
- [8] Beckermann C and Viskanta R 1988 *Int. J. Heat Mass. Transfer* **31** 2077-2089
- [9] Beckermann C and Viskanta R 1989 *Chemical Eng. Communications* **85** 135-156
- [10] Kharicha A, Stefan-Kharicha M, Ludwig A and Wu M 2012 MCWASP XII to be print
- [11] Worster M G 1992 *J. Fluid Mech.* **237** 649-669
- [12] Beckermann C, Fan C and Mihailovic J 1991 *Int. Video J. of Eng. Res.* **1** 71-82
- [13] Li J, Wu M, Hao J and Ludwig A 2012 *Comp. Mater. Sci.* **55** 407-418
- [14] Li J, Wu M, Hao J, Kharicha A and Ludwig A 2012 *Comp. Mater. Sci.* **55** 419-429
- [15] Wu M and Ludwig A 2007 *Metall Mater Trans A* **38** 1465
- [16] Bear J 1972 *Dynamics of fluids in porous media* (New York, USA: American Elsevier)
- [17] Drummond J E and Tahir M I 1984 *Int. J. Multiph. Flow* **10** 515-540